Academic Journal of Science and Technology
ISSN: 2771-3032 | Vol. 22, No. 1, 2026

Structural Parameter Optimization and Far-Field Characteristics of GaN-Based Micro-LEDs for RGB Emission Using FDTD Simulation

Wei Luo, Miao He, Deping Xiong

Guangdong University of Technology, Guangzhou, 510006, China

Abstract: As the core light source for next-generation display technology, Micro-LEDs' light extraction efficiency (LEE) and far-field distribution characteristics directly determine display performance. However, existing research has primarily focused on parameter optimization for a single wavelength (blue light), lacking a systematic analysis of wavelength dependence across the RGB color system. In this paper, based on Ansys Lumerical FDTD Solutions and employing a multipole averaging method, we systematically investigated the structural optimization and far-field characteristics of GaN-based Micro-LEDs with a pixel diameter of 3 μm at three wavelengths: 460 nm (blue light), 530 nm (green light), and 620 nm (red light). The main work and conclusions include: (1) By comparing the LEE under conditions with 1–20 dipoles, it was determined that 12 dipoles can achieve stable convergence for all three wavelengths, and it was found that the LEE for red light is generally about 15–20% higher than that for blue light. (2) Based on cavity interference theory, the p-GaN thickness (50–500 nm) was scanned for each of the three colors, yielding optimal thicknesses of 190 nm (blue), 200 nm (green), and 260 nm (red), respectively, and revealing the wavelength-dependent pattern of interference peak position shifts. (3) By scanning sidewall angles from 0° to 60°, the optimal angles for the three colors were determined to be 32° (blue light), 36° (green light), and 30° (red light), with peak LEE_top values reaching 0.60, 0.66, and 0.69, respectively, which are highly consistent with existing research. (4) By comparing the far-field distributions with and without five pairs of TiO_2/SiO_2 DBR sidewall reflectors, we found that the DBRs increased the peak intensity by 72% for blue light and 31% for red light, but provided almost no gain for green light, revealing the differing effects of DBR angle dependence on different wavelengths. This study provides wavelength-dependent optimization guidelines for the pixel structure design of full-color Micro-LED displays.

Keywords: Micro-LED; Light Extraction Efficiency; FDTD Simulation; Sidewall Inclination Angle; Far-field distribution.

1. Introduction

As a new type of self-emissive display technology, Micro-LED is considered the core light source for next-generation display technology due to its advantages of high brightness, high contrast, low power consumption, and long lifespan [1]. These characteristics give Micro-LED broad application prospects in fields such as augmented reality (AR), virtual reality (VR), wearable devices, automotive displays, and high-end televisions [2]. For full-color display applications, RGB Micro-LED pixels are required. While the InGaN material system is typically used for blue and green light emission, significant progress has also been made in recent years in the development of InGaN red Micro-LEDs [3].

However, Micro-LED displays still face several challenges. When pixel sizes are reduced to the micrometer scale, the sidewall effect becomes particularly pronounced, leading to enhanced sidewall emission, causing optical crosstalk between adjacent pixels, and causing the far-field distribution to deviate from the ideal Lambertian distribution [4]. Furthermore, the high refractive index of GaN (approximately 2.45) causes severe total internal reflection (TIR) at the GaN-air interface, trapping most of the generated photons inside the device until they are absorbed [5].

The external quantum efficiency (EQE) of a Micro-LED is equal to the product of the internal quantum efficiency (IQE) and the light extraction efficiency (LEE). Since LEE is highly sensitive to device geometry, substrate topography, and emission wavelength, its accurate evaluation and optimization are crucial [6]. The finite-difference time-domain (FDTD) method has been widely used to study the optical properties and LEE of GaN-based LED structures [7-9]. Ryu et al. [7] used a 3D FDTD system to study the LEE of GaN-based vertical Micro-LEDs and found that LEE strongly depends on chip shape, dimensions, and p-GaN thickness. Vögl et al. [8] investigated the effects of pixel design and emission wavelength on light extraction, revealing that the optimal sidewall angle for different colors ranges from 35° to 40°. Hu Xinpei et al. [9] designed an omnidirectional reflector (ODR) to achieve sidewall-free emission in Micro-LEDs, resulting in a 2.24-fold increase in LEE. However, existing studies have largely focused on optimization for a single wavelength, and systematic comparative studies across three colors remain scarce.

Based on FDTD simulations, this paper systematically optimizes the structural parameters of GaN-based Micro-LEDs for RGB emission. The optimal p-GaN thickness and sidewall angle for each wavelength were determined, and the effects of DBR sidewall reflectors and Ag reflectors on the far-field distribution were analyzed separately. This study provides wavelength-dependent design guidelines for full-color Micro-LED displays.

2. Simulation Theory and Methods

2.1. FDTD method

The FDTD method solves for the distribution of electromagnetic fields by discretizing Maxwell's equations in both space and time [10]. The electric and magnetic fields are interlaced in space and updated alternately in time, subject to the Courant stability condition. A Perfectly Matched Layer (PML) is used as the absorption boundary condition at the computational domain boundary to prevent boundary reflections from affecting simulation accuracy. Since this experiment uses circular pixels, which exhibit rotational symmetry, a two-dimensional planar simulation is adopted to simplify the simulation process.

2.2. Device Structure

The simulation uses a flip-chip Micro-LED structure, as shown in Fig 1 (a). The layer structure from bottom to top is as follows: a 100-nm Ag reflector, a 100-nm ITO layer, a P-GaN layer (variable thickness), a 100-nm InGaN/GaN multi-quantum well (MQW) active layer, and a 2.5-µm N-GaN layer. The distance between the monitor and the device is λ. Light is extracted from the n-GaN surface. The refractive index parameters of the materials at the three colors' wavelengths are shown in Table 1.

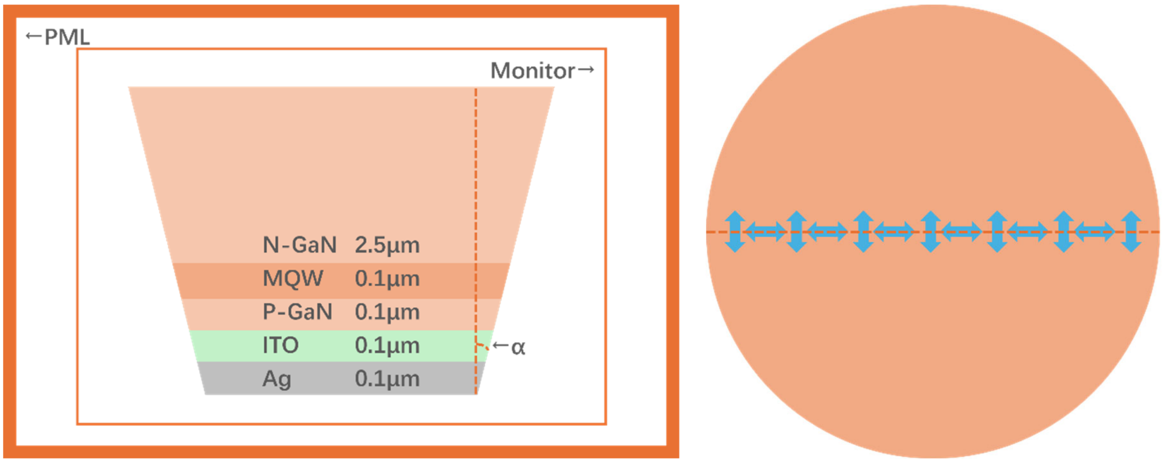

(a) (b)

Figure 1. (a)Schematic Diagram of the Simulation Structure; (b) Schematic Diagram of Dipoles Position

Table 1. Refractive Index of Materials

λ	Ag	ITO	GaN	MQW	SiO2	TiO2
460nm	0.143392	2.022100	2.470250	2.577260	1.464850	2.788070
530nm	0.129331	1.940500	2.413570	2.462700	1.460820	2.670210
620nm	0.131030	1.866800	2.383000	2.402590	1.457420	2.591490

2.3. Definition of LEE

The wavelength-resolved LEE_totoal and LEE_top are defined as:

$$LEE_{total}(\lambda) = T(\lambda) = \frac{P_{monitor(\lambda)}}{P_{source(\lambda)}}$$
$$LEE_{top}(\lambda) = T_{top}(\lambda) = \frac{P_{top(\lambda)}}{P_{source(\lambda)}} \qquad (2\text{-}1)$$

Here, T is the transmittance of the FDTD power monitor, T_top is the transmittance at the top of the FDTD power monitor, P_monitor is the total optical power detected by the monitor, P_top is the optical power detected by the top monitor, and P_source is the total radiated power of the dipole. The central wavelengths of the dipole light sources are set to 460 nm (blue), 530 nm (green), and 630 nm (red), respectively.

2.4. Multipole Averaging Method

Electric dipole sources are uniformly distributed throughout the active layer of the MQW, representing spatially incoherent luminescence generated by electron-hole recombination. Since this experiment employs two-dimensional planar simulation, we consider only dipoles uniformly distributed along a single diameter within the MQW plane; their positions and polarization directions are shown in Fig 1(b). After simulating each dipole independently, we take the arithmetic mean:

$$LEE_{pixel} = \frac{\sum LEE_i}{N} \qquad (2\text{-}2)$$

Here, N represents the number of dipoles. Only in-plane (TE) polarized dipoles are considered, since InGaN quantum wells primarily emit TE-polarized light.

2.5. Far-Field Transformation

The far-field radiation distribution was obtained via a Fourier transform of the near-field data and calculated using Lumerical's built-in functions. Far-field intensity:

$$I(\theta) = |E\_far(\theta)|^2 \qquad (2\text{-}3)$$

The range of θ is from -90° to +90°.

3. Simulation Parameter Settings and Convergence Analysis

3.1. FDTD Settings

The key parameters for the FDTD simulation are shown in

Table 2.

Table 2. Key Parameters for FDTD Simulation

Parameters	Setting Value
Grid Size	5 nm(MQW) 10 nm(others)
Simulation Time	1000 fs
Number of PML layers	8

3.2. Convergence of the Number of Dipoles

The LEE was calculated for 1–20 dipoles at different diameters (1–10 μm) across three wavelengths. The results are shown in Fig 2 (due to the high density of data points, the data was visualized for easier analysis by grouping radii in pairs from smallest to largest and shifting them sequentially by 0.5 along the Y-axis). Stable convergence was achieved for all three wavelengths with as few as 12 dipoles, with the error between adjacent wavelengths being less than 5%. Blue light is most sensitive to the number of dipoles at small pixel sizes (d < 3 μm), while red light exhibits the most stable convergence.

Based on the convergence analysis results, d = 3 μm and N = 12 were selected as the reference parameters for subsequent optimization. After removing the y-axis offset used for visualization, the actual LEE values for different diameters ranged from 0.45 to 0.90, with red light consistently exceeding blue light by approximately 15–20%.

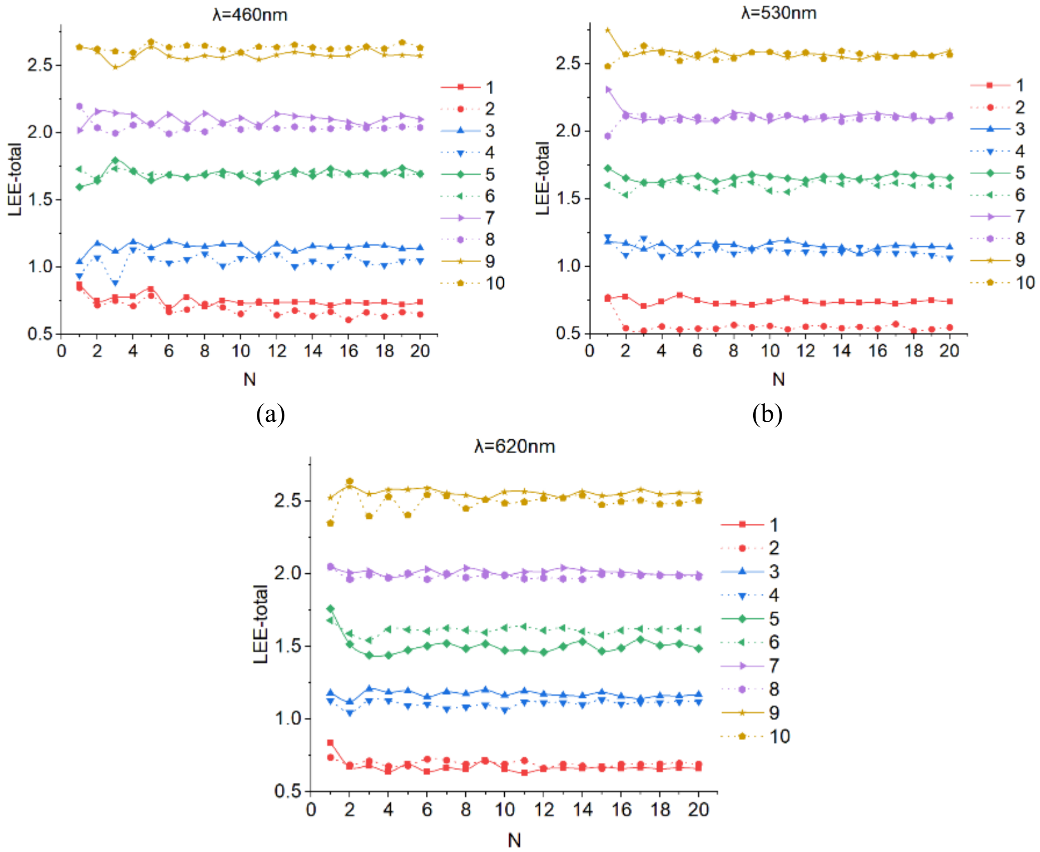

(c)

Figure 2. Variation of LEE with the Number of Dipoles for Different Diameters. λ=460nm; (b) λ=530nm; (c) λ=620nm

4. Optimization of P-GaN Thickness

4.1. Theory of Cavity Interference

The light emitted by the MQW interferes with the light reflected by the Ag mirror, forming an optical cavity. The conditions for constructive interference are:

$$2nd = K\frac{\lambda}{2} \tag{4-1}$$

Here, d is the distance from the MQW to the Ag mirror, n is the refractive index, and K is an integer.

4.2. Results

The P-GaN thickness was scanned from 50 nm to 500 nm in 10-nm increments. The FDTD results are shown in Fig 3, where the LEE exhibits distinct periodic oscillations, confirming the cavity interference effect. Theoretically, any P-GaN thickness at the wave peak could be selected; however, considering that P-GaN cannot be too thin in actual manufacturing processes, P-GaN thicknesses of 190 nm (λ = 460 nm), 200 nm (λ = 530 nm), and 260 nm (λ = 620 nm) were chosen for subsequent experiments.

5. Optimization of Sidewall Inclination Angle

5.1. Physical Mechanism

The inclined sidewall redirects the light path by altering the total internal reflection (TIR) conditions at the n-GaN–air interface. Light that would otherwise be trapped by TIR can be redirected into the escape cone. There is an optimal angle: if the angle is too small (<10°), the redirecting effect is limited; if it is too large (>50°), the light-emitting area at the top surface decreases.

5.2. Results

The side-wall emission angle α was scanned from 0° to 60° in 2° increments, while simultaneously recording LEE_top (forward emission) and LEE_total (omnidirectional). The results are shown in Figure 4. For red light, LEE_total was the highest (0.85), but LEE_top was not the highest (0.64), indicating that side-wall emission accounts for a significant proportion. For display applications, LEE_top should be the primary optimization target, as side-wall emission causes crosstalk between pixels. Subsequent experiments should select the angles α corresponding to the maximum LEE_top values at different wavelengths, namely 32° (λ = 460 nm), 36° (λ = 530 nm), and 30° (λ = 620 nm).

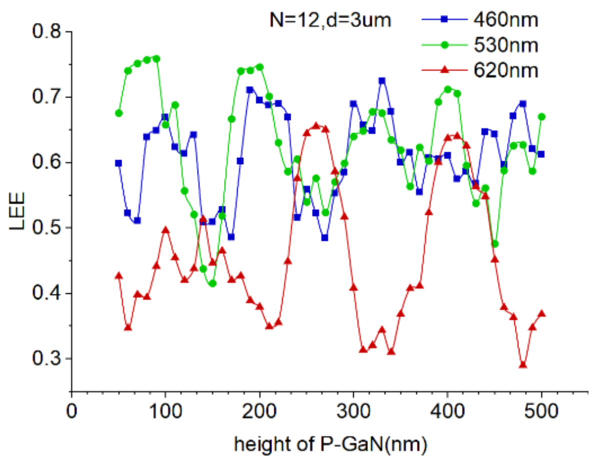

Figure 3. Variation of LEE with P-GaN Height at Different Wavelengths

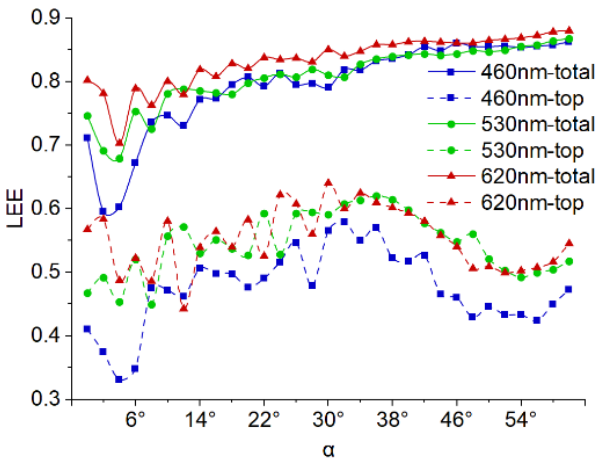

Figure 4. Variation of LEE with Angle α at Different Wavelengths

6. Analysis of DBR Sidewall Reflectors and Their Far-Field Characteristics

6.1. DBR Structure

Five pairs of TiO_2/SiO_2 distributed Bragg reflectors (DBRs) were deposited on the inclined sidewall, with their center wavelengths matched to the respective emission wavelengths. As shown in Figure 5, the sidewall materials, from the inside out, are 100 nm of SiO_2 followed by 5 pairs of TiO_2/SiO_2. The SiO_2 passivation layer isolates the DBR from the GaN. The thickness of the TiO_2/SiO_2 layers in the DBR structure is:

$$d = \frac{\lambda}{4n} \tag{6-1}$$

Here, d represents the material thickness, and n represents the refractive index at the corresponding wavelength [9]. Substituting the data from Table 1 into the calculation yields the TiO_2/SiO_2 thicknesses shown in Table 3.

Table 3. TiO_2/SiO_2 Thickness Corresponding to Different Wavelengths

λ(nm)	d_TiO2(nm)	d_SiO2(nm)
460	41.25	78.50
530	49.62	90.70
620	59.81	106.35

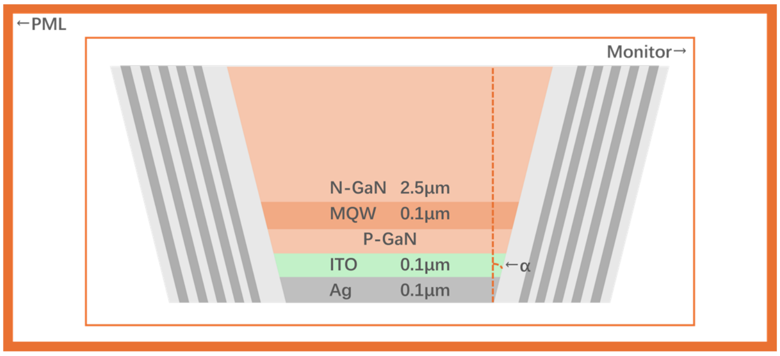

Figure 5. Schematic Diagram of the BDR's Structure

6.2. Far-Field Comparison

A comparison of the far-field distributions with and without the DBR is shown in Figure 6. The DBR introduces a multi-peak interference pattern, resulting in 3–4 distinct interference lobes in the far field (compared to only 1–2 peaks without the DBR). With the DBR, the positions of the three main peaks are concentrated in the range of +15° to +20°, and the directional consistency is somewhat improved.

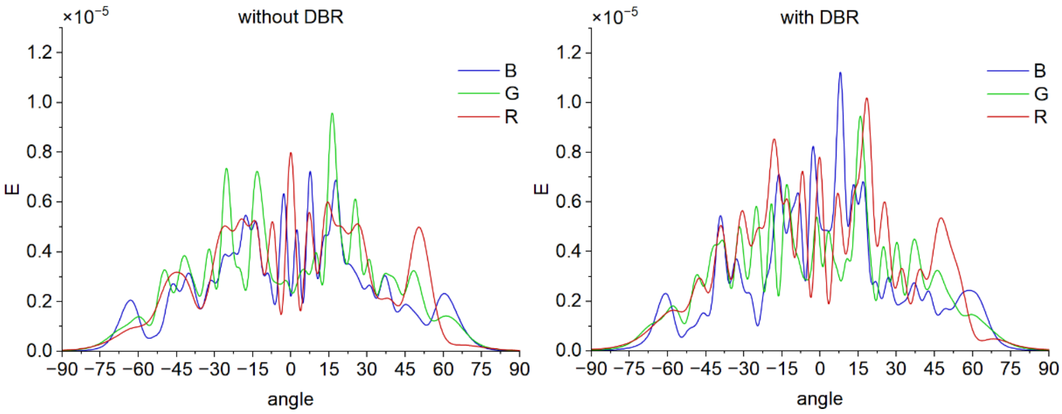

(a) (b)

Figure 6. Schematic Diagram of Far-Field Distribution. (a) without DBR; (b) with DBR

6.3. DBR Angle-Dependence Analysis

The reason for the near-zero gain of green light is attributed to the angle dependence of the DBR on the inclined sidewalls. Since the DBR is coated on sidewalls with an inclination angle of 36°, light is incident at a large angle, causing the DBR reflection band to shift toward the blue and narrow. Furthermore, the reflectance of the p-polarized component drops sharply near the Brewster angle. For green light, the structure itself already achieves a high LEE (0.95×10^{-5}—the highest among the three colors without the DBR), leaving limited room for improvement from the DBR.

7. Summary

Based on FDTD simulations, this paper systematically optimizes the structural parameters of GaN-based Micro-LEDs for RGB tri-color emission. The main conclusions are as follows:

(1) Twelve dipoles can achieve stable LEE convergence for all three wavelengths. The LEE for red light is consistently 15–20% higher than that for blue light, which is attributed to the larger critical angle, lower absorption coefficient, and higher Ag reflectance of red light in GaN.

(2) The optimal P-GaN thicknesses for the three colors are 190 nm (blue), 200 nm (green), and 260 nm (red), respectively.

(3) The optimal sidewall angles for the three colors are 32° (blue), 36° (green), and 30° (red), respectively, with peak LEE_top values reaching 0.60, 0.66, and 0.69, respectively.

(4) The DBR sidewall reflector increases the peak reflectance by 72% for blue light and 31% for red light, but provides almost no gain for green light. This wavelength-dependent behavior is attributed to the angle dependence of the DBR on the tilted sidewall, which causes the reflection band to shift toward the blue.

A summary of the complete optimal structural parameters for the three colors is shown in Table 4.

Table 4. Summary of Optimal Structural Parameters for RGB Micro-LEDs

Parameters	Blue	Green	Red
λ	460nm	530nm	620nm
Pixel Diameter	3μm	3μm	3μm
Number of dipoles	12	12	12
P-GaN Thickness	190μm	200μm	260μm
Sidewall angle α	32°	36°	30°
LEE_top	59.9297%	65.6500%	69.0090%
LEE_total	77.6785%	82.6024%	82.5677%

Future work may include: incorporating radiation recombination distribution weights derived from TCAD electrical simulations to improve the accuracy of LEE calculations; extending the crosstalk analysis to 3×3 arrays; and experimentally verifying the simulation results.

Acknowledgements

This work was supported by the project of sci & tech of Zhongshan (2023A4011).

References

[1] Wu, Y., Ma, J., Su, P., Zhang, L., & Xia, B. (2020). Full-color realization of micro-LED displays. Nanomaterials, 10(12), 2482. https://doi.org/10.3390/nano10122482.

[2] Wu, Y. E., Tsai, C. H., Chen, L. Y., Chen, F. C., & Kuo, H. C. (2025). Current landscape of micro-LED display industrialization. Nanomaterials, 15(9), 693. https://doi.org/10.3390/nano15090693

[3] Pasayat, S. S., Gupta, C., Wong, M. S., et al. (2020). Demonstration of ultra-small (<10 µm) 632 nm red InGaN micro-LEDs with useful on-wafer external quantum efficiency (>0.2%) for mini-displays. Applied Physics Express, 14(1), 011004. https://doi.org/10.35848/apex.14.011004

[4] Li, K. H., Cheung, Y. F., Cheung, W. S., & Choi, H. W. (2015, October 26). Confocal microscopic analysis of optical crosstalk in GaN micro-pixel light-emitting diodes. Applied Physics Letters, 107(17), 171103. https://doi.org/10.1063/1.4934787

[5] Parbrook, P. J., Corbett, B., Han, J., Seong, T.-Y., & Amano, H. (2021). Micro-light emitting diode: From chips to applications. Laser & Photonics Reviews, 15, 2000133. https://doi.org/10.1002/lpor.202000133

[6] Ley, R. T., Smith, J. M., Wong, M. S., Margalith, T., Nakamura, S., DenBaars, S. P., & Gordon, M. J. (2020, June 22). Revealing the importance of light extraction efficiency in InGaN/GaN microLEDs via chemical treatment and dielectric passivation. Applied Physics Letters, 116(25), 251104. https://doi.org/10.1063/5.0013477

[7] Ryu, H. Y., Pyo, J., & Ryu, H. Y. (2020). Light extraction efficiency of GaN-based micro-scale light-emitting diodes investigated using finite-difference time-domain simulation. IEEE Photonics Journal, 12(2), 1-10. https://doi.org/10.1109/JPHOT.2020.2974581

[8] Vögl, F., Avramescu, A., Knorr, F., et al. (2023). Role of pixel design and emission wavelength on the light extraction of nitride-based micro-LEDs. Optics Express, 31(14), 22997. https://doi.org/10.1364/OE.458520

[9] Hu, X. P., Cai, J. H., Ye, Y. Y., et al. (2022). Research on simulation model of high-efficiency GaN-based micro-LED. Acta Optica Sinica, 42(15), 1525001. https://doi.org/10.3788/AOS202242.1525001

[10] Taflove, A., & Hagness, S. C. (2005). Computational electrodynamics: The finite-difference time-domain method (3rd ed.). Artech House.